STRUCTURAL BIOLOGY COMMUNICATIONS

ISSN 2053-230X

The structure of hookworm platelet inhibitor (HPI), a CAP superfamily member from *Ancylostoma caninum*

Dongying Ma, Ivo M. B. Francischetti, Jose M. C. Ribeiro and John F. Andersen*

Laboratory of Malaria and Vector Research, NIH/NIAID, 12735 Twinbrook Parkway, Rockville, MD 20852, USA. *Correspondence e-mail: john.andersen@nih.gov

Received 12 January 2015
Accepted 9 February 2015

Edited by W. N. Hunter, University of Dundee, Scotland

Keywords: antigen V; hemostasis; parasitism.

PDB reference: hookworm platelet inhibitor, 4tpv

Supporting information: this article has supporting information at journals.iucr.org/f

Secreted protein components of hookworm species include a number of representatives of the cysteine-rich/antigen 5/pathogenesis-related 1 (CAP) protein family known as *Ancylostoma*-secreted proteins (ASPs). Some of these have been considered as candidate antigens for the development of vaccines against hookworms. The functions of most CAP superfamily members are poorly understood, but one form, the hookworm platelet inhibitor (HPI), has been isolated as a putative antagonist of the platelet integrins $\alpha_{IIb}\beta_3$ and $\alpha_2\beta_1$. Here, the crystal structure of HPI is described and its structural features are examined in relation to its possible function. The HPI structure is similar to those of other ASPs and shows incomplete conservation of the sequence motifs CAP1 and CAP2 that are considered to be diagnostic of CAP superfamily members. The asymmetric unit of the HPI crystal contains a dimer with an extensive interaction interface, but chromatographic measurements indicate that it is primarily monomeric in solution. In the dimeric structure, the putative active-site cleft areas from both monomers are united into a single negatively charged depression. A potential Lys-Gly-Asp disintegrin-like motif was identified in the sequence of HPI, but is not positioned at the apex of a tight turn, making it unlikely that it interacts with the integrin. Recombinant HPI produced in *Escherichia coli* was found not to inhibit the adhesion of human platelets to collagen or fibrinogen, despite having a native structure as shown by X-ray diffraction. This result corroborates previous analyses of recombinant HPI and suggests that it might require post-translational modification or have a different biological function.

1. Introduction

Helminth species secrete a large number of proteins that play a role in invasion, feeding and modulation of the host immune system. Prominent among these are members of the cysteine-rich secretory/antigen 5/pathogenesis-related 1 (CAP) protein family, which in hookworms are known as *Ancylostoma*-secreted proteins (ASPs; Asojo, 2011; Asojo *et al.*, 2005; Borloo *et al.*, 2013; Gibbs *et al.*, 2008; Mason *et al.*, 2014; Osman *et al.*, 2012). In the medically important hookworms *A. caninum* and *Necator americanus*, many of the most highly abundant, transcriptionally upregulated proteins secreted by the invasive L3 stage are ASP proteins, suggesting that these play a role in parasite establishment in the host (Datu *et al.*, 2008). Two particularly prominent forms, ASP-1 and ASP-2, have been considered as potential hookworm vaccine antigens and other forms have been studied from additional helminth species for similar reasons (Bethony *et al.*, 2005; McSorley & Loukas, 2010; Pearson *et al.*, 2012). A positive correlation between the presence of anti-ASP-2 antibodies in immunized animals and a lack of heavy infestation has been observed, and

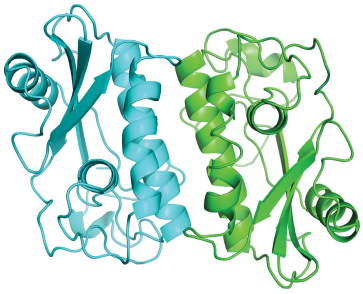

Table 1
Crystallization.

Method	Hanging-drop vapour diffusion
Plate type	Linbro 24-well
Temperature (K)	273
Protein concentration (m*M*)	1
Buffer composition of protein solution	10 m*M* Tris–HCl pH 8.0
Composition of reservoir solution	30% PEG 6000, 0.1 *M* HEPES pH 7.0
Volume and ratio of drop	2 µl, 1:1 ratio
Volume of reservoir (ml)	0.8

in the same study immunization with ASP-2 from *N. americanus* was shown to be protective in laboratory models (Bethony *et al.*, 2005).

CAP superfamily proteins are broadly distributed in eukaryotes, but the vast majority of them have not been functionally characterized. Neutrophil inhibitory factor (NIF) and hookworm platelet inhibitor (HPI) are secreted CAP superfamily members from *A. caninum* that have been associated with specific functions. NIF has been shown to block neutrophil adhesion to endothelial cells by binding to the I domain of the integrin receptor CD11a/CD18 expressed on the neutrophil surface (Moyle *et al.*, 1994; Muchowski *et al.*, 1994). Hookworm-derived HPI was identified as an inhibitor of platelet activation acting through a blockade of the fibrinogen receptor integrin $\alpha_{IIb}\beta_3$ and the collagen receptor integrin $\alpha_2\beta_1$ (Chadderdon & Cappello, 1999; Del Valle *et al.*, 2003). However, recombinant protein failed to inhibit platelet function. Tablysin-15, a CAP-domain protein from the saliva of the blood-feeding horse-fly *Tabanus yao*, has also been shown to modulate platelet and endothelial cell function by binding to integrins $\alpha_{IIb}\beta_3$ and $\alpha_V\beta_3$ *via* an Arg-Gly-Asp (RGD) sequence (Ma *et al.*, 2011; Xu *et al.*, 2012). Additionally, this protein contains a hydrophobic channel as part of its structure that is selective for binding of cysteinyl leukotrienes and may serve to regulate the inflammatory state and vascular tone of the host (Xu *et al.*, 2012).

Structurally, the CAP domain is characterized by an α/β core that is quite highly conserved despite a large degree of sequence variation within the family. This is followed by a hinge region, with a second cysteine-rich C-terminal domain known as the CRISP domain also being present in vertebrate forms (Gibbs *et al.*, 2008). Previously characterized helminth ASP structures only possess the CAP domain and hinge region (Asojo, 2011; Asojo *et al.*, 2005; Borloo *et al.*, 2013; Mason *et al.*, 2014). In this study, we describe the three-dimensional structure of HPI from *A. caninum*, which can be used to help to clarify the role of this protein in the biology of the organism and to understand any structural features that may underlie the reported activity of the protein as an integrin-targeting inhibitor of platelet activation.

2. Materials and methods

2.1. Macromolecule production

A cDNA encoding HPI with a six-histidine tag at the C-terminus was prepared synthetically (BioBasic Inc.), cloned into the expression vector pET-17b and then transformed into *Escherichia coli* strain BL21(DE3)pLysS. For the production of inclusion bodies, LB medium was inoculated with a 10% volume of a saturated culture of the expression strain. After growth at 37°C to an optical density of 0.8, IPTG was added to a concentration of 1 m*M* and the cultures were grown for an additional 3 h at 37°C. After pelleting, washing and freezing, the cells were lysed by sonication of the suspended pellet in 20 m*M* Tris–HCl pH 7.5, 150 m*M* NaCl and the resulting inclusion-body pellet was washed with 1% Triton X-100 in the same buffer, dissolved in 6 *M* guanidine hydrochloride pH 8.0 and reduced by adding DTT to a concentration of 10 m*M*. This solution was then refolded by adding it dropwise with stirring to an excess volume of 20 m*M* Tris–HCl pH 8.0, 0.3 *M* arginine, 1 m*M* EDTA, 0.2 m*M* GSSG, 1 m*M* GSH. After 48 h at 4°C, the protein was concentrated by ultrafiltration. The protein showed relatively good solubility in the refolding buffer, indicating a high yield of native material. Therefore, we skipped the metal-affinity purification step and applied the concentrated material directly onto a Sephacryl S-100 (16/60) column in order to remove aggregated material. A second step of ion-exchange chromatography on Mono Q yielded highly purified, apparently monomeric protein. After purification, the protein was dialyzed against 20 m*M* Tris–HCl pH 7.4, 150 m*M* NaCl. The oligomeric state of the recombinant HPI was determined by gel-filtration chromatography on Superdex 75 using an elution buffer consisting of 20 m*M* Tris–HCl pH 7.5, 0.15 *M* NaCl.

Table 2
Data collection and processing.

Values in parentheses are for the outer shell.

Diffraction source	Beamline 22-ID, APS
Wavelength (Å)	0.97931
Temperature (K)	100
Detector	MAR CCD 300 mm
Crystal-to-detector distance (mm)	175.0
Rotation range per image (°)	1.0
Total rotation range (°)	220
Exposure time per image (s)	1.0
Space group	$P2_1$
a, *b*, *c* (Å)	39.16, 51.98, 73.94
α, β, γ (°)	90, 90.1, 90
Mosaicity (°)	0.522
Resolution range (Å)	30–1.6
Total No. of reflections	174768
No. of unique reflections	39309
Completeness (%)	99.2 (92.1)
Multiplicity	4.4 (3.6)
$\langle I/\sigma(I)\rangle$	11.1 (3.4)
$R_{r.i.m.}$† (%)	8.6 (37.2)
Overall *B* factor from Wilson plot (Å^2)	12.4

† $R_{r.i.m.}$ was estimated by multiplying the R_{merge} value by the factor $[N/(N-1)]^{1/2}$, where N is the data multiplicity.

2.2. Crystallization

The purified HPI was crystallized using the hanging-drop vapour-diffusion method with 30% PEG 6000, 0.1 *M* HEPES pH 7.0. The crystals grew as clusters; the clusters were broken apart with a probe and single-crystal fragments were then

flash-cooled in precipitant solution containing 10% glycerol (Table 1).

2.3. Data collection and processing

Diffraction data were collected on beamline 22-ID of the Southeast Regional Collaborative Access Team (SER-CAT) facility at the Advanced Photon Source (APS), Argonne National Laboratory. Data obtained at 100 K were integrated, merged and scaled using *HKL*-2000 (Otwinowski & Minor, 1997). Data-collection and processing statistics are given in Table 2.

2.4. Structure solution and refinement

The structure of HPI was determined by molecular replacement with *Phaser* (McCoy *et al.*, 2007) using the structure of Na-ASP-2 (PDB entry 1u53; Asojo *et al.*, 2005) from *N. americanus* as a search model. The molecular-replacement solution contained two molecules in the asymmetric unit and was refined by rigid-body refinement in *REFMAC*5 (Murshudov *et al.*, 2011) to give an $R_{\rm cryst}$ of 43% and an $R_{\rm free}$ of 47%. The HPI model was completed by numerous rebuilding and refinement cycles using *phenix.refine* (Afonine *et al.*, 2012) and *Coot* (Emsley *et al.*, 2010). The quality of the model was evaluated using *MolProbity* (Chen *et al.*, 2010). Statistics of data collection and refinement are given in Table 3.

2.5. Platelet-adhesion assays

Platelet-rich plasma was obtained under informed consent from medication-free platelet donors participating in a National Institutes of Health Institutional Review Board-approved protocol of the Department of Transfusion Medicine (DTM/NIH, Blood Bank). For platelet-adhesion assays, platelet-rich plasma was incubated with calcein-AM (2 µ*M*, Calbiochem) for 30 min at room temperature and centrifuged in the presence of EDTA (5 m*M*) and apyrase (0.2 units ml^{-1}). Platelets were resuspended (2 × 10^5 µl^{-1}) in Tyrode's buffer (no additions; Francischetti *et al.*, 1997). Inhibition of platelet adhesion to immobilized collagen was examined by fluorometry. Microfluor Black microtiter 96-well plates (Thermo Labsystems, Franklin, Massachusetts, USA) were coated with 50 µl (1 µg per well in phosphate-buffered saline; PBS) of fibrillar (Horm) or soluble collagen I (BD Biosciences) or fibrinogen (50 µg per well) overnight at 4°C in PBS pH 7.4. Wells were washed with PBS and blocked with 2%(*w*/*v*) BSA (in PBS). Calcein-labeled platelets (2 × 10^5 µl^{-1}) were incubated with HPI or EDTA for 20 min, and 50 µl of platelets was

Table 3
Structure solution and refinement.

Resolution range (Å)	28.81–1.60
Completeness (%)	99.2
No. of reflections, working set	37332
No. of reflections, test set	1980
Final $R_{\rm cryst}$ (%)	15.7
Final $R_{\rm free}$ (%)	19.7
No. of non-H atoms	
Protein	2852
Water	370
Total	3222
R.m.s. deviations	
Bonds (Å)	0.008
Angles (°)	1.08
Average *B* factors (Å^2)	
Protein	15.6
Water	28.1
Ramachandran plot	
Most favored (%)	97.4
Allowed (%)	100
PDB code	4tpv

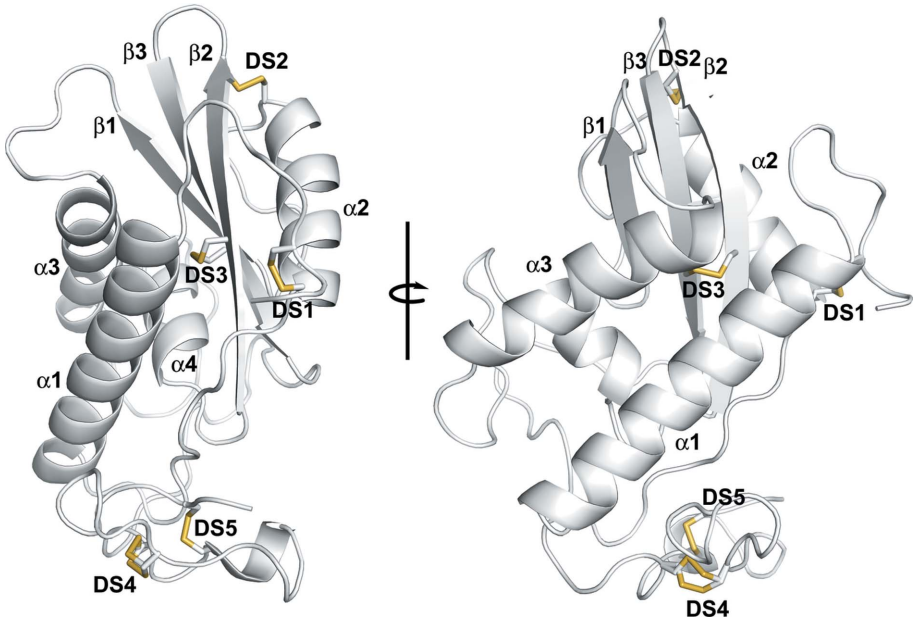

Figure 1
Ribbon diagram of the HPI model. The left and right panels are related by a rotation of approximately 90° around the axis shown. α-Helices are labeled α1–α4 and β-strands are labeled β1–β3. The disulfide bonds discussed in the text are labeled DS1–DS5.

Figure 2
Structural relationships among ASPs. Structure-based alignment of HPI with Na-ASP-2 from *N. americanus* (PDB entry 1u53; Asojo *et al.*, 2005), Ac-ASP-7 from *A. caninum* (second domain, PDB entry 3nt8; Asojo, 2011) and Oo-ASP-1 from *Ostertagia ostertagi* (PDB entry 4g2u; Borloo *et al.*, 2013). The CAP1–CAP4 motifs are highlighted in green. Conserved disulfide bonds 1–5 are highlighted in black. The two histidine positions found in the 'active-site' cleft are marked by hash marks and the candidate disintegrin motifs are marked by asterisks. The consensus sequences for CAP1–CAP4 in PROSITE nomenclature are as follows: CAP1, [GDER][HR][FYWH][TVS][QA][LIVM][LIVMA]Wxx[STN]; CAP2, [LIVMFYH][LIVMFY]XC-[NQRHS]Yx[PARH]x[GL]N[LIVMFYWDN]; CAP3, HNxxR; CAP4 G[EQ]N[ILV] (Gibbs *et al.*, 2008).

added to each well. After 1 h, the wells were washed three or four times with Tyrode-BSA and adhesion was estimated by fluorescence (excitation at 485 nm and emission at 530 nm).

3. Results and discussion

3.1. The structure of HPI

Recombinant HPI (3–187) containing a C-terminal histidine tag was crystallized in space group $P2_1$ with two monomers in the asymmetric unit (Fig. 1). Each monomer consists of an $\alpha/\beta/\alpha$ structure typical of CAP-domain proteins, as well as a shorter C-terminal hinge region (Fig. 1). The secondary-structural elements of the protein are arranged similarly to other ASPs with the pattern $\alpha1$–$\alpha2$–$\beta1$–$\alpha3$–$\alpha4$–$\beta2$–$\beta3$ (Fig. 1). The protein is stabilized by five disulfide bonds that are equivalent to the conserved disulfides contained in other members of the CAP superfamily, as shown in the structure-based alignment in Fig. 2. Three of these disulfides lie in the CAP domain itself and link Cys7 to Cys48 of $\alpha2$ (disulfide bond 1), Cys61 of $\alpha2$ to Cys129 of $\beta2$ (disulfide bond 2) and Cys124 of $\beta2$ to Cys137 of $\beta3$ (disulfide bond 3) (Figs. 1 and 2). The C-terminal hinge region of HPI then begins at the conserved residue Gly154 [part of the conserved GX(PV) motif] and is similar in conformation to other ASP proteins (Gibbs *et al.*, 2008). It is stabilized by two conserved disulfide bonds linking Cys157 to Cys169 (disulfide bond 4) and Cys160 to Cys178 (disulfide bond 5) (Figs. 1 and 2). Based on the ASP-categorization system of Osman *et al.* (2012), HPI belongs to the group 3 ASPs, since it is missing two conserved histidine residues characteristic of group 1 ASPs that lie in the loop between $\alpha2$ and $\beta1$ and on helix $\alpha4$ (Osman *et al.*, 2012; Asojo *et al.*, 2005, 2011; Assumpção *et al.*, 2013; Mason *et al.*, 2014). These two residues have been suggested to form a metal-binding site lying at the base of a cleft that could be involved in the hypothesized proteolytic activities of CAP-domain proteins or in the copper-dependent superoxide dismutase activity reported for a CAP-domain protein from the saliva of the blood-feeding insect *Dipetalogaster maxima* (Asojo *et al.*, 2005, 2011; Assumpção *et al.*, 2013; Mason *et al.*, 2014). In HPI, the two histidine residues are replaced by Pro65 and Asn110 (Fig. 2). Group 2 ASPs differ from group 1 and 3 proteins in that they lack disulfide bond 2 shown in the amino-acid sequence alignment in Fig. 2.

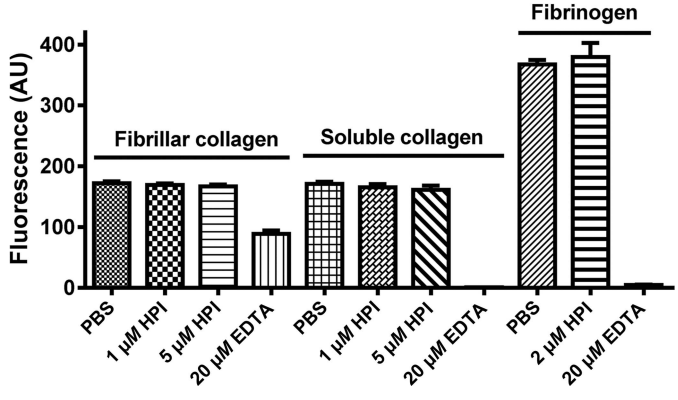

Figure 3
Adhesion of platelets to collagen and fibrinogen in the presence and absence of HPI. Microtiter plates coated with fibrillar collagen, soluble collagen or fibrinogen were blocked with BSA and exposed to calcein-labeled platelets that had been pre-incubated with HPI for 20 min. After 1 h, the plate was washed and adhesion was measured by fluorescence.

Based on previous comparative studies, two amino-acid sequence motifs, designated CAP1 and CAP2, have been catalogued in the PROSITE database (Sigrist *et al.*, 2012) and shown to be diagnostic for members of the CAP superfamily (Fig. 2). These conserved motifs lie in the region of the cleft containing the two 'active-site' histidine residues of group 1 ASPs (Gibbs *et al.*, 2008). Recently, the CAP1 consensus sequence has been expanded to include additional conserved residues, most notably a highly conserved cysteine lying C-terminal to the originally described motif (Borloo *et al.*, 2013). HPI shows only partial conservation of the expanded CAP1, with 11 of 15 residues matching the consensus, while CAP2 adheres to the consensus at six of nine positions. Two additional motifs, CAP3 and CAP4, have more recently been described by Gibbs *et al.* (2008). HPI matches the consensus for CAP3 at all five positions and that for CAP4 at three of four positions.

3.2. Assessment of integrin-binding function

Extracts of *A. caninum* have been shown to prevent the aggregation and adhesion of platelets in response to a variety of agonists, including collagen, ADP, thrombin and epinephrine, suggesting the presence of an inhibitor that blocks integrin interactions with activating ligands (Chadderdon & Cappello, 1999; Del Valle *et al.*, 2003). HPI was originally isolated from extract preparations based on its ability to inhibit the binding of fibrinogen and collagen to their respective platelet integrins $\alpha_{IIb}\beta_3$ and $\alpha_2\beta_1$ (Del Valle *et al.*, 2003). Inhibitory integrin-binding proteins known as

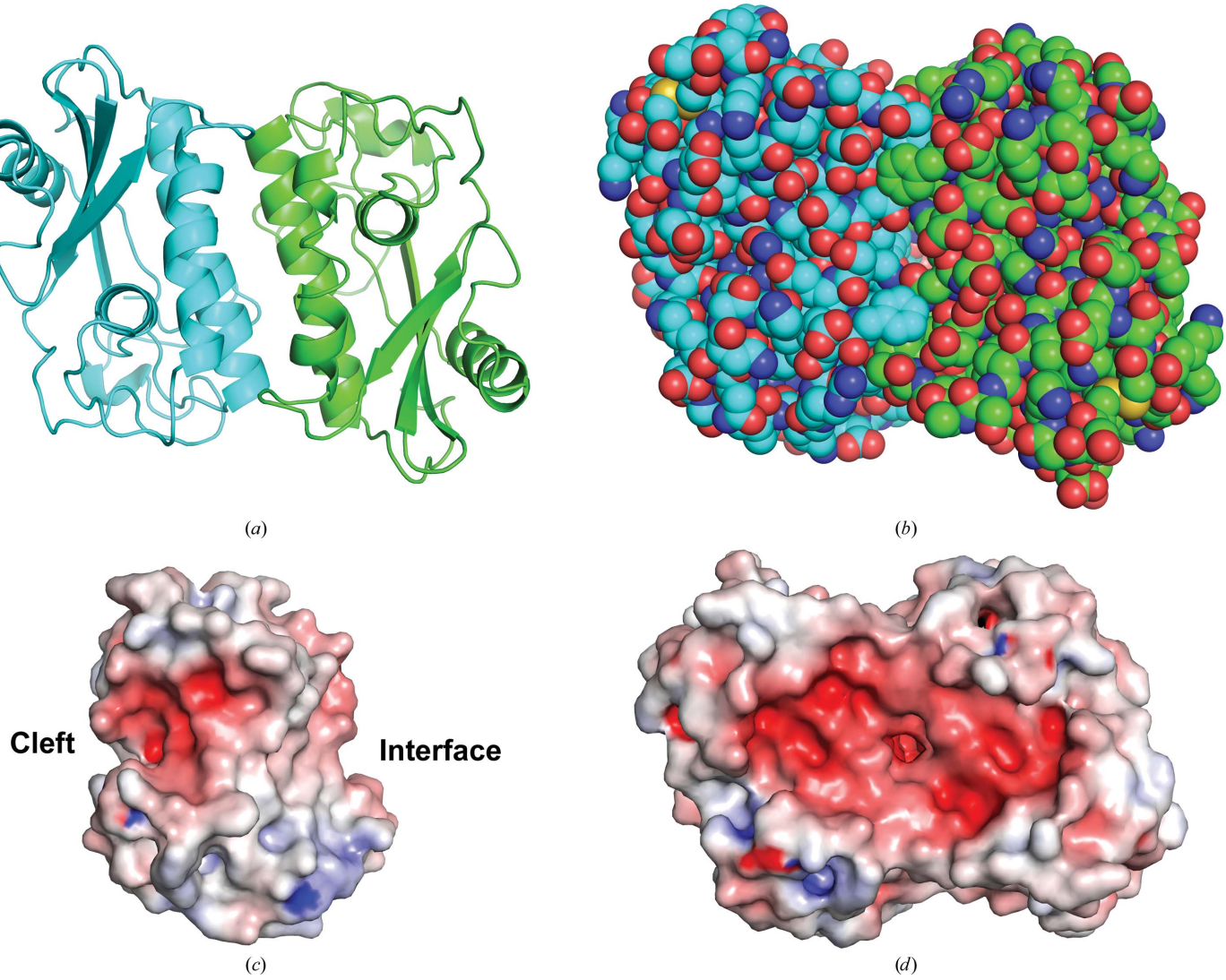

Figure 4
Oligomeric state and electrostatic surface properties of HPI. (*a*) Ribbon diagram of the dimeric structure of the asymmetric unit with chain *A* colored green and chain *B* colored cyan. The two molecules are related by a twofold rotation axis perpendicular to the plane of the page. The dimer interface is made up primarily of elements of α1 and α3. (*b*) Space-filling diagram of the model from (*a*) showing packing of the interface. (*c*) Electrostatic map of the surface of the HPI monomer. Negatively charged surface areas are colored red and positively charged areas are colored blue. The dimer interface and negatively charged cleft are labeled. (*d*) Electrostatic map of the HPI dimer showing the joining of the anionic surfaces of HPI monomers into a large, negatively charged depression.

disintegrins derived from snake venoms and other sources contain an Arg-Gly-Asp (RGD) sequence motif or a variant of this sequence that has been proven to be the primary integrin–inhibitor interaction site (Assumpcao *et al.*, 2012; Wermelinger *et al.*, 2009). The structures of integrins $\alpha_{IIb}\beta_3$ and $\alpha_v\beta_3$ in complex with Arg-Gly-Asp peptides reveal that the residues of the motif interact with the head structure of the integrin in a groove located between the α and β subunits (Xiao *et al.*, 2004; Xiong *et al.*, 2002). Inhibitors containing the motif normally present a projecting loop containing a tight turn with the RGD sequence at its apex. The only CAP-domain protein with a confirmed integrin-inhibitory function is the horse-fly salivary protein tablysin-15, which possesses an RGD sequence at the apex of a tight turn lying in an N-terminal extension of the CAP domain (Xu *et al.*, 2012). Two possible disintegrin motifs related to RGD are present in the HPI sequence (Fig. 2), with the most likely being Lys144-Gly145-Asp146 (KGD; Assumpcao *et al.*, 2012). The KGD motif is a known active variant of RGD and occurs in the sequence of HPI at a location that is C-terminal to β3 at the beginning of the hinge region. It does not, however, lie at the apex of a tight turn as in tablysin-15. Rather, the lysine side chain is buried and the aspartate, while on the surface, does not appear to project sufficiently to interact with the integrin. The second possible motif, Lys37-Thr38-Ser39 (KTS; Marcinkiewicz *et al.*, 2003), has been shown to interact with integrin $\alpha_1\beta_1$ in other proteins and lies near the beginning of α1. This sequence is also not completely exposed and does not appear to be oriented in a manner consistent with integrin interaction.

Table 4
Hydrogen-bonding and salt-bridge interactions at the dimer interface in HPI.

Chain *B* residue	Distance (Å)	Chain *A* residue
Arg34 NH1	3.17	Glu19 OE1
Lys37 NZ	3.13	Asp16 OD1
Asn81 ND2	2.93	Asn35 OD1
Trp91 NE1	2.95	Asn88 OD1
Glu23 OE1	2.68	Arg34 NE
Glu23 OE2	2.69	Arg34 NH2
Asn35 OD1	3.02	Asn81 ND2
Asn88 OD1	3.06	Trp91 NE1
Asp172 O	2.89	Gln174 NE2

Recombinant HPI produced after isolation and cloning has been reported by Del Valle *et al.* (2003) to be unable to block the adhesion of platelets to either collagen or fibrinogen, suggesting a possible folding problem with the recombinant material produced in *E. coli*. We have tested the refolded recombinant protein used for this study for its ability to block platelet adhesion to collagen and fibrinogen. While the crystal structure shows that the protein is properly folded, no inhibition of the adhesion of calcein AM-loaded platelets to soluble collagen, fibrillar collagen or fibrinogen was observed (Fig. 3), indicating that the *E. coli*-produced protein is inactive. This suggests that HPI may require removal of the His-tag modification, may require additional post-translational

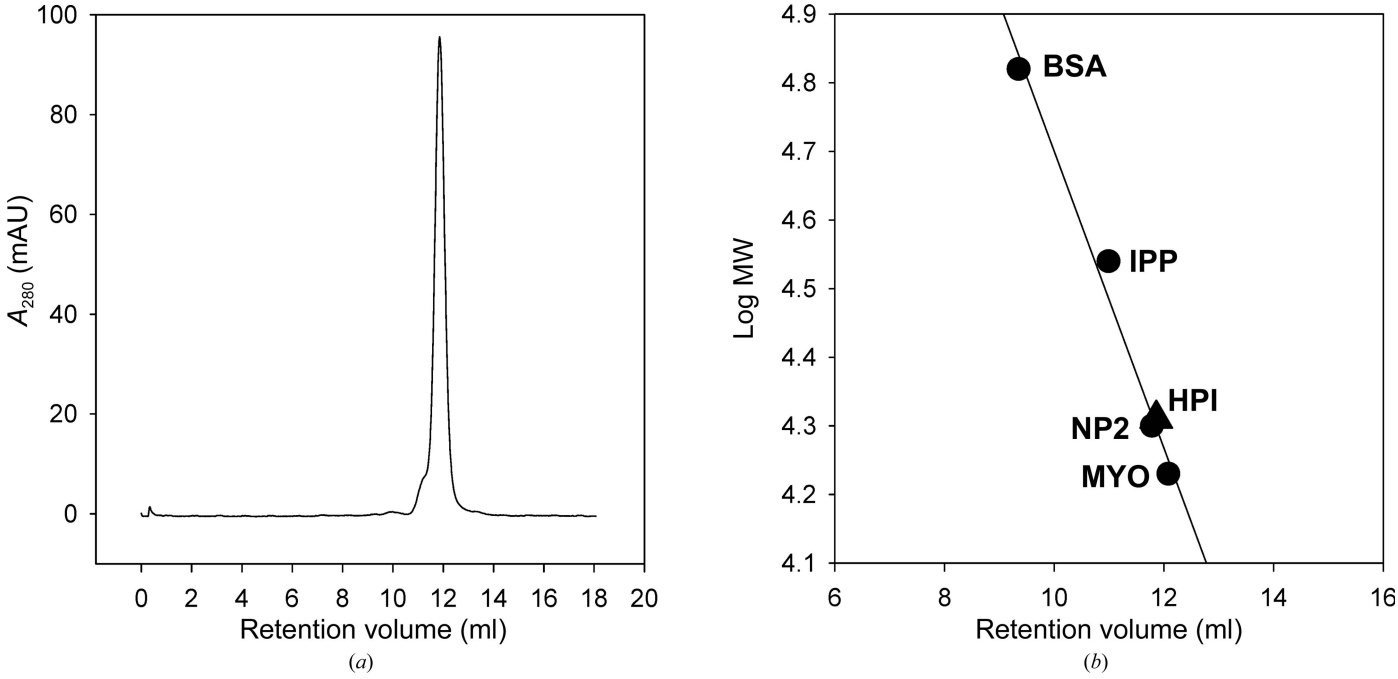

Figure 5
Solution oligomeric state of HPI. (*a*) Recombinant HPI was applied onto a Superdex 75 (10/300) column and eluted with 20 m*M* Tris–HCl pH 7.5, 150 m*M* NaCl. (*b*) A series of standard proteins were chromatographed on the same column in the same buffer system: bovine serum albumin (BSA; 66.1 kDa), *Rhodnius prolixus* inositol polyphosphate phosphatase (IPP; 34.7 kDa), nitrophorin 2 (NP2; 19.9 kDa) and horse heart myoglobin (MYO; 17 kDa). The elution volume and calculated mass of the HPI monomer are also indicated with a triangle. The results indicate that HPI is monomeric under these conditions.

modification for activation or may have a different biological function than suggested to this point.

3.3. Oligomeric state of HPI

The two HPI monomers contained in the asymmetric unit are related by a rotation around a twofold axis that runs approximately perpendicular to the longitudinal axes of α1 and α3 in both molecules (Figs. 4*a* and 4*b*). The contact interface consists of a four-helix bundle made up of α1 and α3 from each monomer. The interface, as determined by analysis with *PISA* (Krissinel & Henrick, 2007), is relatively large, with 1117 Å^2 of surface (per monomer) being buried, and has a calculated interaction energy (ΔG) of -10.1 kcal mol^{-1}. A notable surface feature of the HPI monomer is a large negatively charged patch that lies directly adjacent to the interaction interface and includes the cleft corresponding to that containing the two conserved histidine residues found in group 1 ASPs as well as other CAP-domain proteins (Fig. 4*c*). In the dimeric model, the negatively charged areas belonging to each of the two monomers align almost perfectly to form a negatively charged surface depression that measures approximately 38 Å across in its longest dimension (Fig. 4*d*). The dimer interface contains a number of hydrogen-bond and electrostatic interactions between the two chains, which are listed in Table 4. Although *PISA* calculations suggest that the dimer would be stable in solution, gel-filtration chromatography on Superdex 75 indicated that recombinant HPI remains largely monomeric in an elution-buffer system containing 150 m*M* sodium chloride, making the relevance of the dimeric form uncertain (Fig. 5).

Acknowledgements

The authors thank D. Garboczi and A. Gittis for discussions and Van Pham for technical assistance. We also thank the staff of the Southeast Regional Collaborative Access Team, Advanced Photon Source, Argonne National Laboratory for assistance with X-ray data collection. Use of the Advanced Photon Source beamlines was supported by the US Department of Energy, Office of Science, Office of Basic Energy Sciences under contract No. W-31-109-Eng-38. This work was supported by the intramural research program of the NIAID, National Institutes of Health.

References

Afonine, P. V., Grosse-Kunstleve, R. W., Echols, N., Headd, J. J., Moriarty, N. W., Mustyakimov, M., Terwilliger, T. C., Urzhumtsev, A., Zwart, P. H. & Adams, P. D. (2012). *Acta Cryst.* D**68**, 352–367.
Asojo, O. A. (2011). *Acta Cryst.* D**67**, 455–462.
Asojo, O. A., Goud, G., Dhar, K., Loukas, A., Zhan, B., Deumic, V., Liu, S., Borgstahl, G. E. & Hotez, P. J. (2005). *J. Mol. Biol.* **346**, 801–814.
Asojo, O. A., Koski, R. A. & Bonafé, N. (2011). *Acta Cryst.* D**67**, 847–855.
Assumpção, T. C. F., Ma, D., Schwarz, A., Reiter, K., Santana, J. M., Andersen, J. F., Ribeiro, J. M. C., Nardone, G., Yu, L. L. & Francischetti, I. M. B. (2013). *J. Biol. Chem.* **288**, 14341–14361.
Assumpcao, T. C. F., Ribeiro, J. M. C. & Francischetti, I. M. B. (2012). *Toxins*, **4**, 296–322.
Bethony, J., Loukas, A., Smout, M., Brooker, S., Mendez, S., Plieskatt, J., Goud, G., Bottazzi, M. E., Zhan, B., Wang, Y., Williamson, A., Lustigman, S., Correa-Oliveira, R., Xiao, S. & Hotez, P. J. (2005). *FASEB J.* **19**, 1743–1745.
Borloo, J., Geldhof, P., Peelaers, I., Van Meulder, F., Ameloot, P., Callewaert, N., Vercruysse, J., Claerebout, E., Strelkov, S. V. & Weeks, S. D. (2013). *Acta Cryst.* D**69**, 493–503.
Chadderdon, R. C. & Cappello, M. (1999). *J. Infect. Dis.* **179**, 1235–1241.
Chen, V. B., Arendall, W. B., Headd, J. J., Keedy, D. A., Immormino, R. M., Kapral, G. J., Murray, L. W., Richardson, J. S. & Richardson, D. C. (2010). *Acta Cryst.* D**66**, 12–21.
Datu, B. J. D., Gasser, R. B., Nagaraj, S. H., Ong, E. K., O'Donoghue, P., McInnes, R., Ranganathan, S. & Loukas, A. (2008). *PLoS Negl. Trop. Dis.* **2**, e130.
Del Valle, A., Jones, B. F., Harrison, L. M., Chadderdon, R. C. & Cappello, M. (2003). *Mol. Biochem. Parasitol.* **129**, 167–177.
Emsley, P., Lohkamp, B., Scott, W. G. & Cowtan, K. (2010). *Acta Cryst.* D**66**, 486–501.
Francischetti, I. M. B., Saliou, B., Leduc, M., Carlini, C. R., Hatmi, M., Randon, J., Faili, A. & Bon, C. (1997). *Toxicon*, **35**, 1217–1228.
Gibbs, G. M., Roelants, K. & O'Bryan, M. K. (2008). *Endocr. Rev.* **29**, 865–897.
Krissinel, E. & Henrick, K. (2007). *J. Mol. Biol.* **372**, 774–797.
Ma, D., Xu, X., An, S., Liu, H., Yang, X., Andersen, J. F., Wang, Y., Tokumasu, F., Ribeiro, J. M. C., Francischetti, I. M. B. & Lai, R. (2011). *Thromb. Haemost.* **105**, 1032–1045.
Marcinkiewicz, C., Weinreb, P. H., Calvete, J. J., Kisiel, D. G., Mousa, S. A., Tuszynski, G. P. & Lobb, R. R. (2003). *Cancer Res.* **63**, 2020–2023.
Mason, L., Tribolet, L., Simon, A., von Gnielinski, N., Nienaber, L., Taylor, P., Willis, C., Jones, M. K., Sternberg, P. W., Gasser, R. B., Loukas, A. & Hofmann, A. (2014). *Int. J. Biochem. Cell Biol.* **50**, 146–155.
McCoy, A. J., Grosse-Kunstleve, R. W., Adams, P. D., Winn, M. D., Storoni, L. C. & Read, R. J. (2007). *J. Appl. Cryst.* **40**, 658–674.
McSorley, H. J. & Loukas, A. (2010). *Parasite Immunol.* **32**, 549–559.
Moyle, M., Foster, D. L., McGrath, D. E., Brown, S. M., Laroche, Y., De Meutter, J., Stanssens, P., Bogowitz, C. A., Fried, V. A., Ely, J. A., Soule, H. R. & Vlasuk, G. P. (1994). *J. Biol. Chem.* **269**, 10008–10015.
Muchowski, P. J., Zhang, L., Chang, E. R., Soule, H. R., Plow, E. F. & Moyle, M. (1994). *J. Biol. Chem.* **269**, 26419–26423.
Murshudov, G. N., Skubák, P., Lebedev, A. A., Pannu, N. S., Steiner, R. A., Nicholls, R. A., Winn, M. D., Long, F. & Vagin, A. A. (2011). *Acta Cryst.* D**67**, 355–367.
Osman, A., Wang, C. K., Winter, A., Loukas, A., Tribolet, L., Gasser, R. B. & Hofmann, A. (2012). *Biotechnol. Adv.* **30**, 652–657.
Otwinowski, Z. & Minor, W. (1997). *Methods Enzymol.* **276**, 307–326.
Pearson, M. S., Tribolet, L., Cantacessi, C., Periago, M. V., Valerio, M. A., Jariwala, A. R., Hotez, P., Diemert, D., Loukas, A. & Bethony, J. (2012). *J. Allergy Clin. Immunol.* **130**, 13–21.
Sigrist, C. J. A., de Castro, E., Cerutti, L., Cuche, B. A., Hulo, N., Bridge, A., Bougueleret, L. & Xenarios, I. (2012). *Nucleic Acids Res.* **41**, D344–D347.
Wermelinger, L. S., Geraldo, R. B., Frattani, F. S., Rodrigues, C. R., Juliano, M. A., Castro, H. C. & Zingali, R. B. (2009). *Arch. Biochem. Biophys.* **482**, 25–32.
Xiao, T., Takagi, J., Coller, B. S., Wang, J.-H. & Springer, T. A. (2004). *Nature (London)*, **432**, 59–67.
Xiong, J.-P., Stehle, T., Zhang, R., Joachimiak, A., Frech, M., Goodman, S. L. & Arnaout, M. A. (2002). *Science*, **296**, 151–155.
Xu, X., Francischetti, I. M. B., Lai, R., Ribeiro, J. M. C. & Andersen, J. F. (2012). *J. Biol. Chem.* **287**, 10967–10976.